RSC Advances

PAPER

View Article Online
View Journal | View Issue

Cite this: *RSC Adv.*, 2022, **12**, 11974

Novel adamantyl clubbed iminothiazolidinones as promising elastase inhibitors: design, synthesis, molecular docking, ADMET and DFT studies†

Atteeque Ahmed,[a] Aamer Saeed,*[a] Syeda Abida Ejaz,*[b] Mubashir Aziz,[b] Muhammad Zaffar Hashmi,[c] Pervaiz Ali Channar,[aj] Qamar Abbas,[d] Hussain Raza,[e] Zahid Shafiq[f] and Hesham R. El-Seedi[ghi]

Porcine Pancreatic Elastase (PPE) is a serine protease that is homologous to trypsin and chymotrypsin that are involved in various pathologies like inflammatory disease, Chronic Obstructive Pulmonary Disease (COPD), acute respiratory distress syndrome, cystic fibrosis, and atherosclerosis. PPE if remained uninhibited would lead to digestion of important connective tissue. We developed new structurally diverse series of adamantyl-iminothiazolidinone hybrids to divulge elastase inhibition assay. To identify potent derivatives, *in silico* screening was conducted and *in vitro* studies disclosed that the compounds **5a**, **5f**, **5g**, and **5h** showed excellent binding energies and low IC_{50} values. *In silico* studies including molecular docking, DFT studies (using the B3LYP/SVP basis set in the gas phase) drug likeness scores and molecular dynamic simulation studies were conducted to evaluate protein–ligand interactions and to determine the stability of top ranked conformation. *In silico* studies further supported the results of *in vitro* experiments and suggest these derivatives as novel inhibitors of elastase enzyme.

Received 29th December 2021
Accepted 24th March 2022

DOI: 10.1039/d1ra09318e

rsc.li/rsc-advances

Introduction

Elastase is a pancreatic enzyme that is resistant to degradation in the gastrointestinal tract. It is made by pancreatic acinar cells. Its measurement in faeces has been widely used to determine pancreatic exocrine adequacy because to its simplicity; nonetheless, it is insensitive to mild to moderate pancreatic insufficiency.[1,2] It is initially synthesized as an inactive zymogen before being activated by trypsin in the duodenum. Reduced faecal elastase concentrations have been seen in various gastrointestinal illnesses (*e.g.*, duodenal enteropathy), in circumstances where elastase is destroyed by bacteria (*e.g.*, inflammatory bowel disease), and as a consequence of diarrhea's dilution effect.[3] Because the test looks for human elastase, it does not react with the pancreatic enzyme replacement drug derived from swine that is used to treat cystic fibrosis. Elastin is also present in the skin's bottom layer, alongside collagen, as well as nerves, blood arteries, lymph nodes, and muscles.[4] Collagen is a fundamental component of the extracellular matrix (ECM) and has a direct impact on the skin. The preservation of collagen structure is linked to the intrinsic and photoaging processes of the skin.[5,6] Elastase are serine proteases that hydrolyze the amides and esters present in many proteins, including elastin. Elastic fibers are composed of elastin, a protein found in the majority of connective tissues and tendons. Because elastase destroys elastic fibers and leads to skin inflammation and other skin-related issues, decreasing elastase activity may be an effective method of avoiding skin ageing.[7] Adamantyl moiety is a non-polar cage structure that provides lipophilic character to the molecule and improves the barrier crossing ability of a molecule to the biological system. In most cases, the adamantyl group tunes the hydrophobicity of the molecule by enhancing the penetrating ability and therapeutic activity of several trial compounds through various mechanisms.[8–10] The steric factor of the adamantyl group promotes the stability and pharmacologic half-life of compounds. From the last

[a]*Department of Chemistry, Quaid-I-Azam University, Islamabad 45320, Pakistan. E-mail: asaeed@qau.edu.pk; aamersaeed@yahoo.com; Fax: +92-51-9064-2241; Tel: +92-51-9064-2128*

[b]*Department of Pharmaceutical Chemistry, Faculty of Pharmacy, The Islamia University of Bahawalpur, Bahawalpur 63100, Pakistan*

[c]*Department of Chemistry, COMSATS University, Islamabad, Pakistan*

[d]*Department of Biology, College of Science, University of Bahrain, Sakhir, Kingdom of Bahrain*

[e]*Department of Biological Sciences, College of Natural Sciences, Kongju National University, 56 Gongjudehak-Ro, Gongju, Chungnam 314-701, Republic of Korea*

[f]*Department of Chemistry, Bahauddin Zakariya University, Bosan Road, Multan, Pakistan*

[g]*School of Food and Biological Engineering, Jiangsu University, Zhenjiang 212013, China*

[h]*International Joint Research Laboratory of Intelligent Agriculture and Agri-Products Processing, Jiangsu Education Department, Jiangsu University, Zhenjiang, China*

[i]*Department of Chemistry, Faculty of Science, Menoufia University, Shebin El-Kom 32512, Egypt*

[j]*Department of Basic Sciences, Mathematics and Humanities, Dawood University of Engineering and Technology, Karachi 74800, Pakistan*

† Electronic supplementary information (ESI) available. See https://doi.org/10.1039/d1ra09318e

few decades, adamantyl appending compounds as potential pharmacophore, attracted the attention of several synthetic chemists and pharmacists.[11] As a result, adamantyl analogs passed from the intensive biological investigation.[12] To date, several marketed drugs incorporating with adamantyl scaffold are now available. Adamantyl-containing compounds exhibit a broad spectrum of biological activities such as antiviral, anti-HIV, antifungal, anti-diabetic, antibacterial,[13] anti-inflammatory,[14] antimicrobial, hypoglycemic activity, treatment of COVID-19,[15,16] and treatment for neurological disease.[17,18]

Acyl thioureas signify a class of pharmaceutically important compounds to develop the architect of a potential drug. These molecules have been explored for many pharmaceutical activities.[19–21] and in agriculture as an insecticide and weed killer. In addition, they are the precursor for the synthesis of a number of heterocyclic compounds and metal complexes[22] Acyl thiourea have also been applied as ion sensors and for the estimation of metal ions.[23–25] These electron-rich molecules act as ligand and organocatalysts in various asymmetric synthesis[26–28]

Heterocyclic skeletons containing five-member rings with two heteroatoms are promising core structures, commonly encountered in organic and medicinal chemistry. Thiazolidinone motifs are biologically significant five-membered heterocycle that is very common substructures in various pharmacological active molecules and known to exhibit a wide range of biological activities such as anticancer, antifungal, anti-inflammatory, antimicrobial, antidiabetic, inhibiting neuraminidase of influenza virus, and anti-HIV,[29] anti-schistosomal activity. Among these are inhibitors for necroptosis, selective GSK-3β inhibitor, anticancer activity,[30] aldose reductase inhibitor,[31] potent antiproliferative agent and inhibitor for non-membrane protein tyrosine phosphate. The aforesaid facts inspired us to synthesize novel ethyl 3-adamantanyl-2-((2-methyl benzoyl)imino)-4-oxothiazolidin-5-ylidene acetates (**5a–j**) for the appraisal of elastase inhibition assay. The structures of some pharmacologically active compounds and designed molecules are shown in Fig. 1.

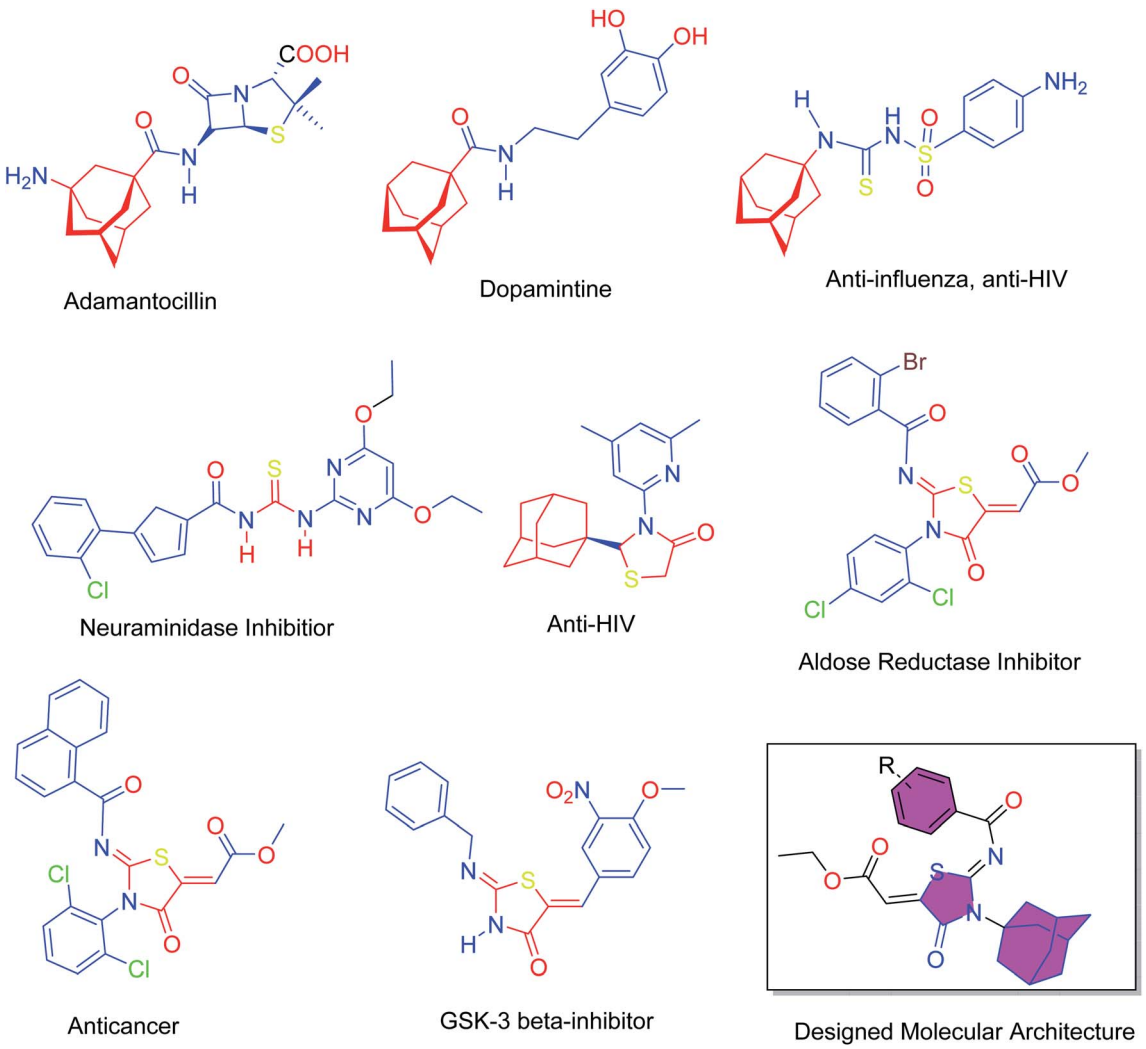

Fig. 1 Pharmacological active compounds containing adamantyl, thiourea, thiazolidinone moieties and the designed molecules.

Results and discussion

The target compounds were synthesized according to synthetic route described in Scheme 1. Suitably substituted benzoic acids were converted to corresponding acid chlorides (**1a–j**) using dichloromethane as solvent. The acid chloride was converted to isothiocyanate by adding potassium thiocyanate in acetone. Reaction of the latter *in situ* with an equimolar amount of amantadine (**2**) afforded the acyl thioureas (**3a–j**). Ethyl 4-ethoxypent-4-en-2-ynoate with (**3a–j**) at room temperature in dry ethanol furnished the desired compounds (**5a–j**) in excellent yields and high purity. The complete structures of synthesized derivatives are given in (Fig. 2).

Structure–activity relationship (SAR) of iminothiazolidinones derivatives

The important SAR features can be deduced from this study. The inhibitory potential of the synthesized amantadine derivatives was investigated using elastase from porcine pancreas. The relationships between different substituted and unsubstituted patterns were analyzed on their ability to inhibit elastase. Such type of analysis assists to infer the SAR among the synthesized screened derivatives. Oleanolic acid is a pentacyclic triterpenoid and has been used as stander. In the current study, amantadine thiazolidinone derivatives were synthesized to find out more effective and selective antagonists of elastase. Among the synthesized analogues, compounds **5a**, **5f**, **5g**, and **5h** were showed high potency against elastase. The presence of unsubstituted phenyl group in **5g**, provide effectiveness to develop high potency against elastase with IC_{50} of 0.124 ± 0.022 μM (Table 1) which is 50 times more potent as compared to oleanolic acid value of 5.996 ± 0.882 μM. With respect to structural comparison compounds with a methyl **5a**, flouro **5f**, chloro **5h**, and bromo **5d** substituted phenyl group exhibit excellent inhibitory activity. This is due to positive mesomeric effect of these substituents. Interestingly the compound **5g** doesn't have any substitution on benzoylimino group of a compound, but it showed excellent IC_{50} value and good binding energy. It can be perceived that absence of mesomeric effect might increase activity against PPE enzyme.

Kinetic mechanism

An inhibition kinetic study was carried out in order to better understand the mode of action of the synthetic compound against elastase. Based on our IC_{50} results, we choose our most potent compound **5g** for further investigation to determine the type of inhibition and the constant of inhibition. $1/V$ *versus* substrate *N*-succinyl-Ala-Ala-*p*-nitroanilide $1/[S]$ in the presence of different inhibitor concentrations was plotted using a Lineweaver–Burk plot in which the results were a series of straight lines; however, the result of a Lineweaver–Burk plot of compound **5g** revealed that V_{max} remained constant without significantly affecting the slopes. While K_m increases with increasing concentration, V_{max} remains constant with only a statistically insignificant difference. A competitive inhibition model was used to explain this behavior (Fig. 3A), and a second plot (Fig. 3B) of slope against concentration of **5g** revealed the E_I dissociation constant. The inhibitor concentration of **5g** was plotted against the slope of the graph, and the calculated K_i value was found to be 0.6 μM.

Computational studies

Quantum chemistry through density functional theory calculation. All the selected molecules (**5a–j**) were optimized

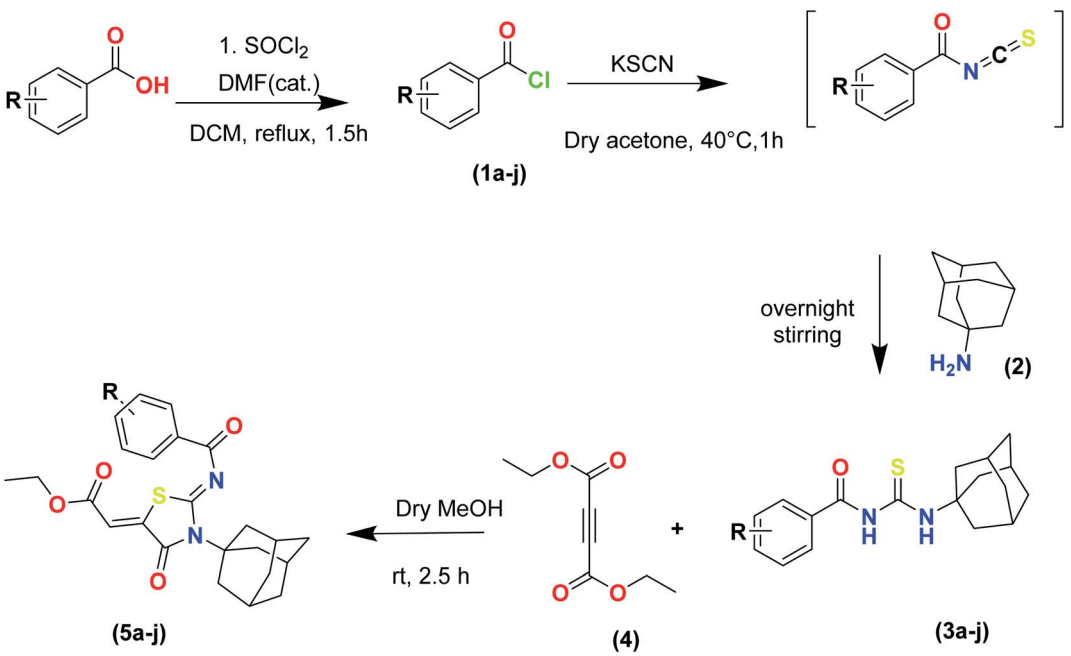

Scheme 1 Synthesis of ethyl (*Z*)-2-((*Z*)-3-((3s,5s,7s)-adamantan-1-yl)-2-((2-methylbenzoyl)imino)-4-oxothiazolidin-5-ylidene)acetates (**5a–j**).

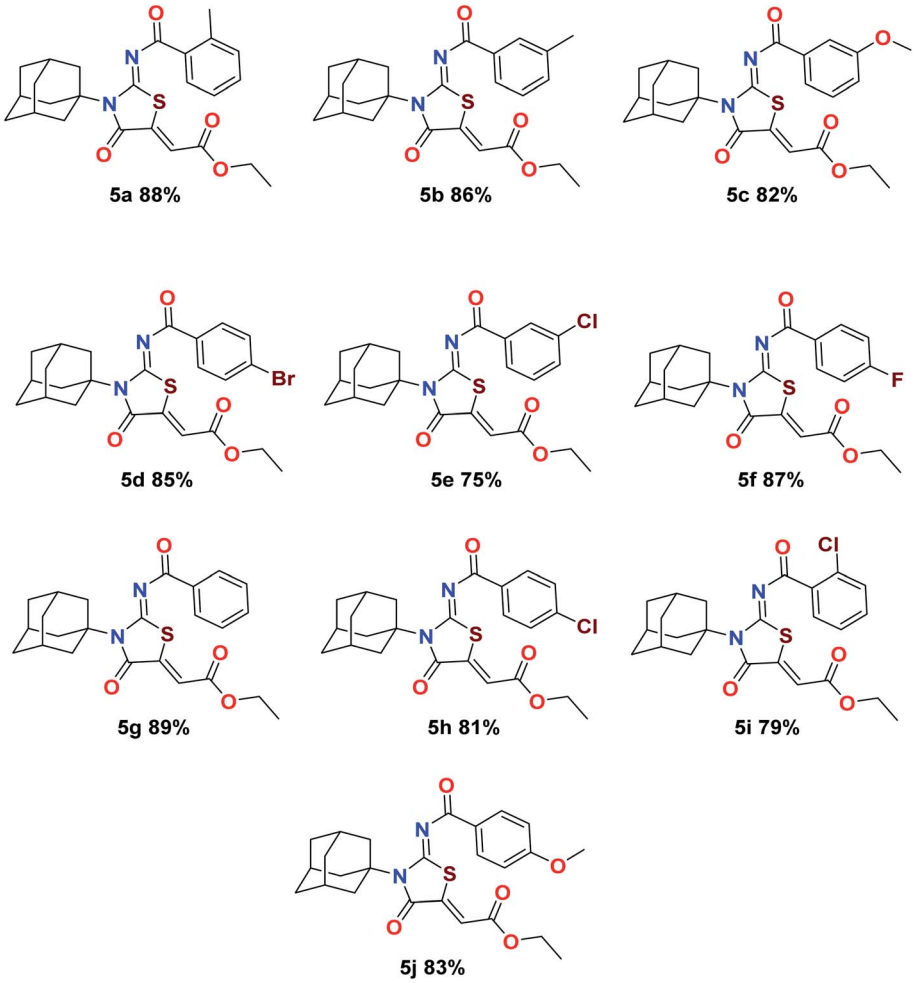

Fig. 2 Molecular structures and percent yields of final compounds (5a–j).

firstly, using the B3LYP/SVP basis set in the gas phase, and their values are shown in Table 2.

The geometries of selected compounds were optimized to lowest energy gradient and no imaginary frequencies were observed which demonstrate that all structures were true local minima. The optimized structures of selected compounds are shown in Fig. 4.

Table 1 Elastase (elastase from porcine pancreas) inhibitory activity of derivatives (5a–j)[a]

Compound	Elastase IC_{50} + SEM (μM)	Compound	Elastase IC_{50} + SEM (μM)
5a	0.854 ± 0.241	**5f**	0.384 ± 0.624
5b	0.982 ± 0.286	**5g**	0.124 ± 0.022
5c	0.738 ± 0.117	**5h**	0.221 ± 0.059
5d	0.597 ± 0.087	**5i**	1.791 ± 0.213
5e	1.961 ± 0.336	**5j**	3.257 ± 0.541
Oleanolic acid	5.996 ± 0.882		

[a] SEM = standard error of the mean; values are expressed in mean ± SEM.

The molecular orbital (MO) analysis is of prime importance in quantum chemistry. It has been broadly defining chemical behavior. The highest occupied molecular orbital (HOMO) and lower unoccupied molecular orbital (LUMO) are the chief molecular orbitals in a compound. They are used to explain chemical properties such as reactivity, stability, and kinetics. The FMO orbitals of synthesized compounds are shown in Fig. 5.

The hardness (η) defined the extent to which a molecule is hard or soft. The softer the molecule, the better will be the reactivity.

Electronegativity (X) characterizes the power to attract electrons. All these properties were estimated at. The compound **5c** showing smallest HOMO–LUMO energy gap value (0.064 eV) predicts a good chemical reactivity. The compound **5j** is showing a small hardness value (0.071), high polarizability thus leading to be the soft molecule among all compounds. The higher the electronegativity value in the case of compound **5d** showing (0.173) value exposes that **5d** has good electron attracting power and acts as a better electrophile among all compounds. While compounds **5f** and **5a** also showed good reactivity after **5c**, with the energy gap values 0.067 eV and

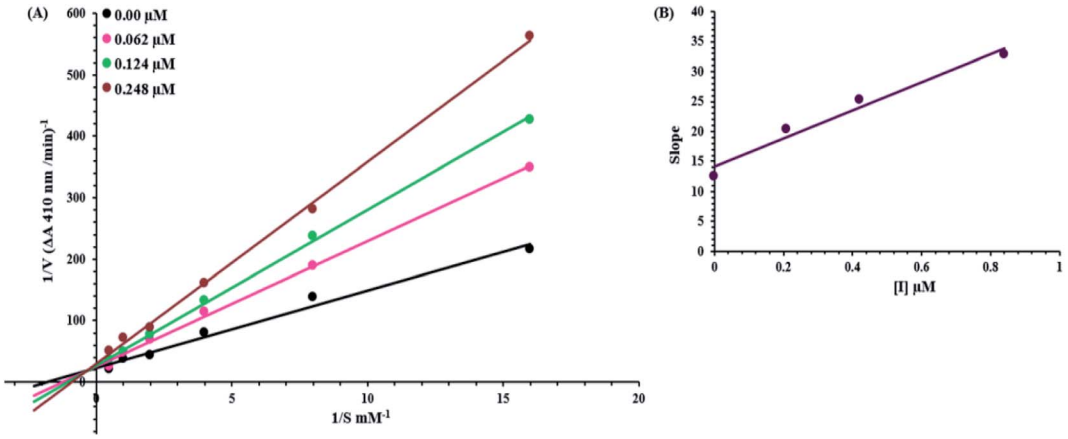

Fig. 3 Lineweaver–Burk plots for inhibition of elastase from porcine pancreas in the presence of compound **5g** (A) concentrations of **5g** were 0.00, 0.062, 0.124 and 0.248 µM, substrate *N*-succinyl-Ala-Ala-Ala-*p*-nitroanilide concentrations were 2, 1, 0.5, 0.25, 0.125 and 0.0625 mM. (B) The insets represent the plot of the slope.

Table 2 Geometric parameters of the compounds (**5a–j**)

		Gas phase		
S. no.	Compound	Optimization energy (hartree)	Polarizability (α) (a.u.)	Dipole moment (Debye)
1	**5a**	−1747.578754	175.593333	2.632463
2	**5b**	−1756.398850	215.067333	2.151600
3	**5c**	−1821.412424	174.135000	1.454307
4	**5d**	−4262.687518	309.789333	1.774701
5	**5e**	−2162.996044	170.469000	1.848393
6	**5f**	−1806.453269	166.362333	1.037827
7	**5g**	−1717.551017	201.042667	1.104426
8	**5h**	−2163.003741	172.960333	2.863819
9	**5i**	−2163.010784	173.656000	2.127731
10	**5j**	−1843.417542	311.708667	4.266993

0.069 eV, respectively. In the same manner, just after **5j** the compounds **5b**, **5g** and **5d** showing high polarizability with the values of 0.072, 0.076 and 0.078, respectively. Energetic parameters of compounds (**5a–j**) are showing in Table 3 below.

Molecular docking studies. Porcine Pancreatic Elastase (PPE) is a serine protease that is homologous to trypsin and chymotrypsin. It is composed of single polypeptide chain of 240 amino acids that are linked with four disulphide linkages. Moreover, it is complexed with Ca^{2+} atom which is necessary for its stability.[32] PPE consist of four subsites, among these most of inhibitors bind to S1 and S2 active sites. S1 site is consider as a primary specificity active site (Fig. 6). PPE plays pivotal role in onset and progression of inflammatory disease like cancer and COPD.[33] PPE if remained uncontrolled would lead to digestion of important connective tissue. Keeping in view the importance of PPE, *in silico* studies were conducted to support the result of *in vitro* assays. Crystallographic structure of PPE was downloaded from Protein data bank. (PDB ID: 1BMA; resolution 1.99). The important amino acids residues of catalytic site were selected and docked with potent thiazolidinone derivatives. The important amino acid residues of PPE protein are as follows; THR221, SER203, HIS60, SER222, PHE223, VAL224, SER225, TRP179, CYS199, GLY201, GLY198, THR152, LEU227, CYS229, ALA104 THR152, GLY228, ARG226, VAL103, SER203, HIS60, and GLN200. Synthesized derivatives were selected on the basis of IC_{50} values obtained during *in vitro* assays. Based on IC_{50} value, **5a**, **5f**, **5g** and **5h** was selected for *in silico* studies as these derivatives showed excellent inhibitory potential during *in vitro* assays.

Synthesized derivatives were evaluated for binding affinities and binding scores with amino acid residues of active pocket. Binding affinities were determined on the basis of predicted inhibitory constant value (k_i). Most of the compounds exhibited potent binding scores and demonstrated good binding affinities. The best conformation of protein–ligand was selected and analyzed further for bonding and non-bonding interactions. Docking scores of potent compounds with their IC_{50} values are given in Table 4.

The detailed 3D and 2D binding interactions of derivative **5a** within active pocket of PPE enzyme is shown in Fig. 7. The amino acid residues involved in bonding and non-bonding interactions with **5a** were THR152, LEU227, CYS229, GLY228,

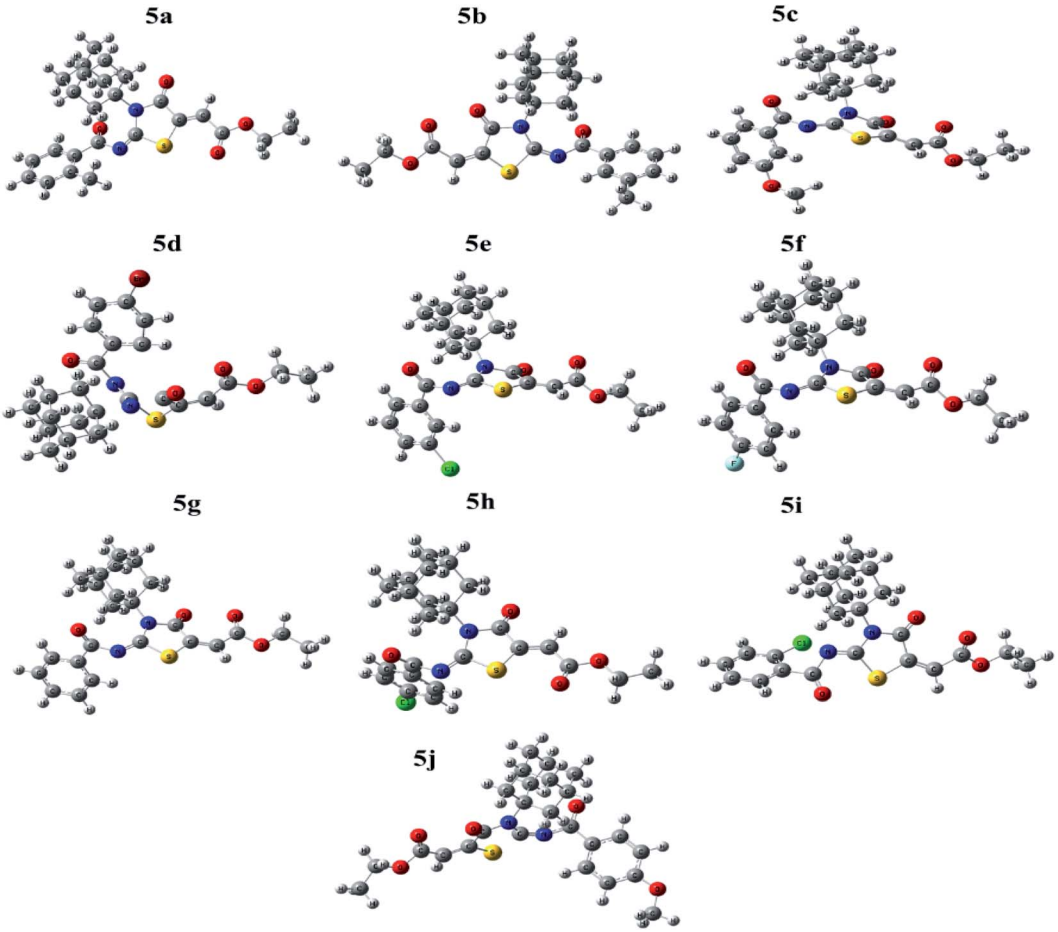

Fig. 4 Optimized structures of the compounds (**5a–j**).

SER225, ARG226, TRP179, VAL103, PHE223, VAL224, SER203, HIS60, SER222 and GLN200. Briefly substituted benzoyl imino ring of parent compound was making strong pi-sulfur linkage with C229. Compound **5a** showed good binding energy and IC_{50} value which might be due to substitution of methyl group on benzoylimino ring. It was observed that compound **5a** was producing hydrogen bonding of moderate strength with GLN200 with bond length of 3.1 Å. Presence of methyl group induce positive mesomeric effect by donating electrons. Moreover, acetate group of molecule was making alkyl and pi-alkyl interactions with PHE223 and VAL103. Amantadine ring was making van der Waals interactions with VAL222 and SER225.

The detailed 3D and 2D binding interactions of derivative **5f** within active pocket of PPE enzyme is shown in Fig. 8. The amino acid residues involved in bonding and non-bonding interactions with **5f** TRP179, SER225, VAL224, PHE223, GLN200, CYS199, SER203, SER222 and ARG226. Briefly flouro substituted benzoylimino ring of parent compound was making strong π–π stacked interaction with PHE223. Compound **5f** showed good binding energy and IC_{50} value which might be due to substitution of fluorine on benzoyl imino ring. Fluorine induce positive mesomeric effect by donating electrons. Moreover, amantadine ring was making alkyl interaction with VAL103. In addition, single hydrogen-acceptor bonding was observed with ARG226 with bond length of 2.9 Å. The van der Waals interactions were exhibited by oxothiazolidinylidene ring with TRP179 and CYS199.

The detailed 3D and 2D binding interactions of derivative **5g** within active pocket of PPE enzyme is shown in Fig. 9. The amino acid residues involved in bonding and non-bonding interactions with **5g** were PHE223, ARG226, VAL103, ASP63, THR100, HIS60, ASP202, SER222, SER203, THR221, GLN200, CYS199 and VAL224. Briefly, compound **5g** was making two hydrogen bonds with VAL224 and GLN200 with bond length of 2.95 Å and 3.21 Å respectively. Interestingly, compound **5g** doesn't bear any substitution on benzoylimino group, but it showed excellent *in vitro* IC_{50} value and exhibited good binding energy during molecular docking studies. It can be predicted that presence of stabilizing hydrogen bonds with good cutoff value might have increased the activity against PPE enzyme. Moreover, central amantadine ring was making hydrophobic interaction with SER222. Other amino acids involved in van der Waals interactions were SER203 and SER103.

The detailed 3D and 2D binding interactions of derivative **5h** within active pocket of PPE enzyme is shown in Fig. 10. The amino acid residues involved in bonding and non-bonding interactions with **5h** were SER225, GLN200, SER203, SER222, HIS60, VAL224, VAL103, PHE223, TRP179 and ARG226. Briefly,

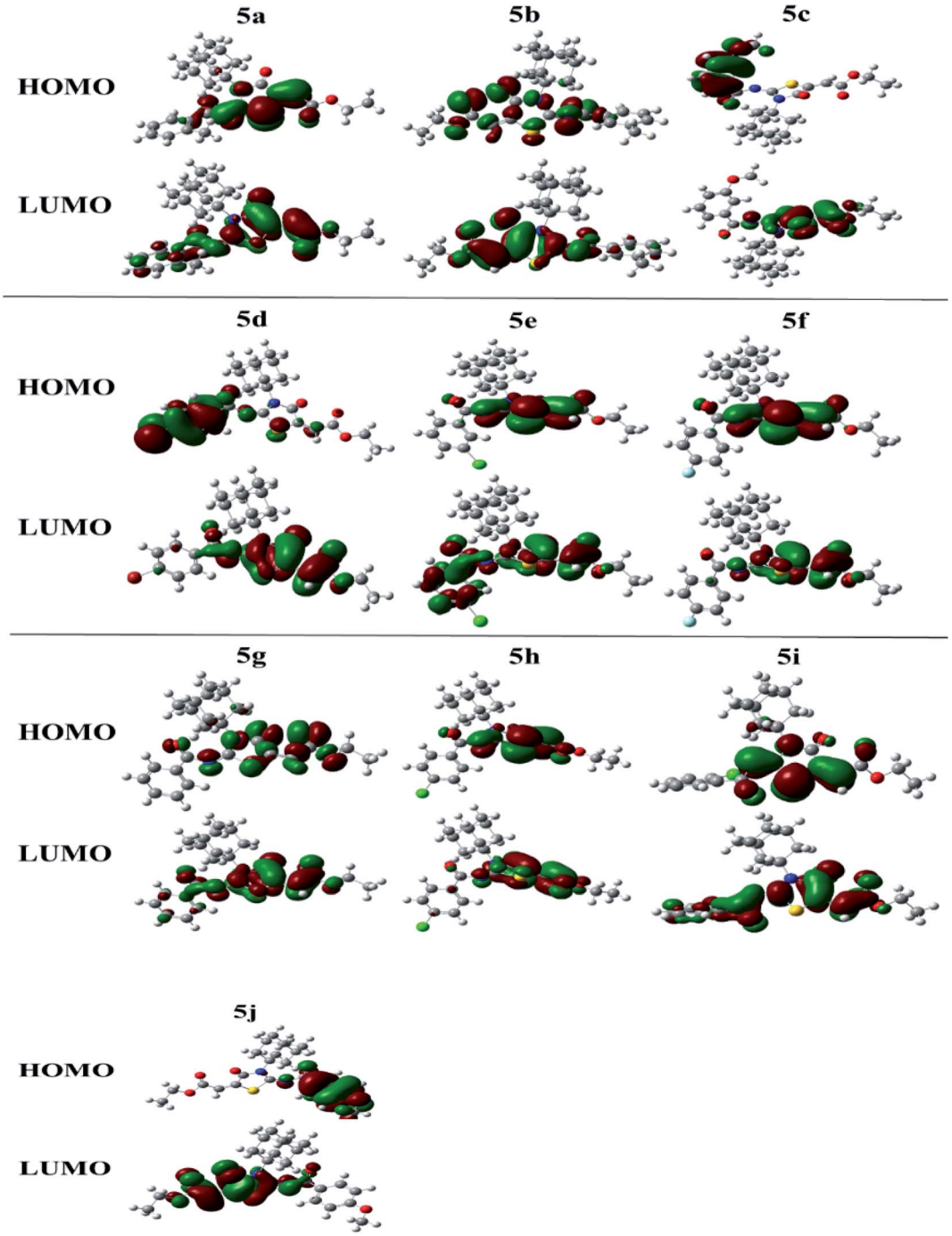

Fig. 5 FMOs of the compounds (**5a–j**).

5h compound is appeared to be most potent derivative which showed highest binding energy of -28.82 kJ mol^{-1} and excellent *in vitro* activity (IC_{50} value). It might be due to substitution of chlorine on benzoyl imino ring of compound. Substituted chlorine was making strong π-alkyl interaction with TRP179. Also, benzoyl imino ring was making π–π stacked interaction with PHE223. Moreover, it was observed that amantadine ring was playing pivotal role in making hydrophobic interactions with amino acid residues f active site. Amantadine ring of **5h** compound was producing π and π-alkyl interaction with VAL103. Whereas acetate group of **5h** compound was involved in π-alkyl interaction with VAL224. Furthermore, compound **5h** was producing hydrogen bond with SER225 having bond length of 2.3 Å. The amino acid residues involved in van der Waals interaction with **5h** compound were GLN200, SER203, SER222 and HIS60.

The co-crystal ligand was re-docked into active pocket of elastase enzyme which was aimed to validate the docking

Table 3 Energetic parameters of the compounds (5a–j)

Compound	E_{HOMO} (eV)	E_{LUMO} (eV)	ΔE_{gap} (eV)	Hardness (η)	Softness (S)	Electronegativity (X)
5a	−0.25326	0.18451	0.069	0.219	2.28	0.034
5b	−0.13569	0.00824	0.127	0.072	6.95	0.064
5c	−0.25591	0.19175	0.064	0.224	2.23	0.032
5d	−0.25186	−0.09513	0.157	0.078	6.38	0.173
5e	−0.26176	0.18998	0.072	0.226	2.21	0.036
5f	−0.25943	0.19229	0.067	0.226	2.21	0.034
5g	−0.13817	0.01304	0.125	0.076	6.61	0.063
5h	−0.26359	0.18141	0.082	0.223	2.25	0.041
5i	−0.26101	0.18360	0.077	0.222	2.25	0.039
5j	−0.23092	−0.08884	0.142	0.071	7.04	0.160

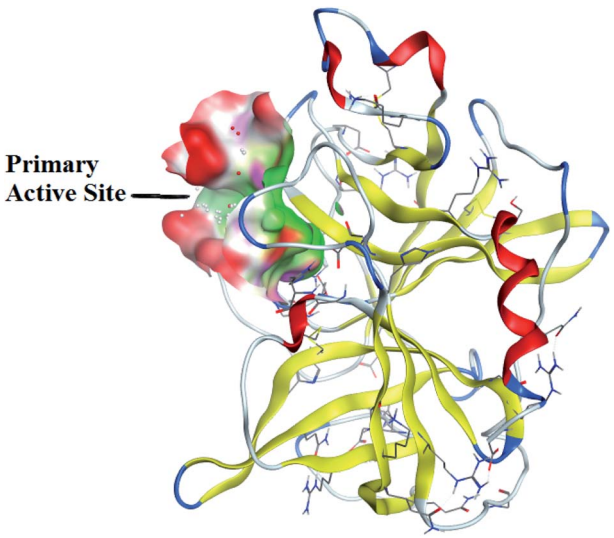

Fig. 6 Crystallographic structure of porcine pancreatic elastase (PPE).

protocol and evaluation of binding score and binding affinity. It was observed that co-crystal ligand was producing important bonding and nonbonding interactions with targeted protein. The amino acid residues which were involved in important stabilizing interactions were THR221, SER203, HIS60, SER222, PHE223, VAL224, SER225, TRP179, GLN200, CYS199, GLY201, GLY198, THR152, LEU227, CYS229, ALA104 and VAL103. Co-crystal ligand was involved in important stabilizing hydrogen bonding with GLN200, VAL224, PHE223 and HIS60. The docking score was found to be −28.03 kJ mol^{-1}. In comparison to synthesized derivatives, it was observed that compound **5h** was producing better docking scores than co-crystal ligand. It can be predicted that synthesized derivatives are better inhibitors of PPE enzyme than co-crystal ligand. The 3D interactions of co-crystal ligand with targeted protein is shown in Fig. 11.

Table 4 Docking score of potent derivatives

Code	Docking score (kJ mol^{-1})	IC_{50} + SEM (μM)	Predicted inhibitory constant (k_i) (μM)
5a	−24.68	0.854 ± 0.241	2.7
5f	−23.61	0.384 ± 0.624	1.95
5g	−23.56	0.124 ± 0.022	1.94
5h	−28.82	0.221 ± 0.059	1.63
Co-crystal ligand benzyl methyl aminimide	−28.03	—	5.9

Molecular dynamic simulations: analysis of RMSD and RMSF. The root mean square deviation (RMSD) is a metric that indicate the average change in displacement of atoms with respect to frame. The value of RMSD can be obtained by analysis of MD trajectory with respect to time. *Y*-Axis of a graph depicts the evolution of protein RMSD and *x*-axis indicate the course of time in nanosecond. The RMSD of ligand, targeted protein and protein ligand complex is shown in Fig. 12.

The RMSD of ligand is plotted by aligning protein–ligand on the reference protein backbone and RMSD of ligand heavy atoms were calculated. Fig. 12 depicts the evolution of RMSD of protein, ligand and protein–ligand complex. The RMSD value of protein ligand shows that complex attained stability initially up to 30 ns and after that it showed fluctuations in RMSD up to 3 angstrom. After 60 ns of simulation time, complex again stability and remained around 2 angstrom which is perfectly acceptable. After 80 ns, complex RMSD dropped to 1.2 angstrom and remained stable around 1.5 angstrom. In case of targeted protein, RMSD value was quite stable and it attained stability after 10 ns and remained stable around 1 angstrom which is perfect. Green line is indicating evolution of ligand RMSD which is showing fluctuations within 2 angstrom and after 80 ns of simulation time, it got stable at 2 angstrom.

The local changes around protein chain are characterize by root mean square fluctuation (RMSF) values. Fig. 13 depicting the RMSF value of residues index of targeted protein.

Peaks sections are showing those residues which fluctuate more during MD simulation. Usually a residue belonging to N and C terminal tends to fluctuate more whereas more compact regions like secondary structures part are more rigids and show less fluctuation. The stability of ligand complexed with protein are indicated by low RMSF values of amino acid residues of binding site. MD simulations demonstrated total 13 hydrogen bonds were produced between ligand and protein. Hydrogen bonds formed during simulations are tabulated in Table 5.

ADMET properties of compounds (5a–j). Prediction of ADMET properties is prime step in the process of drug discovery

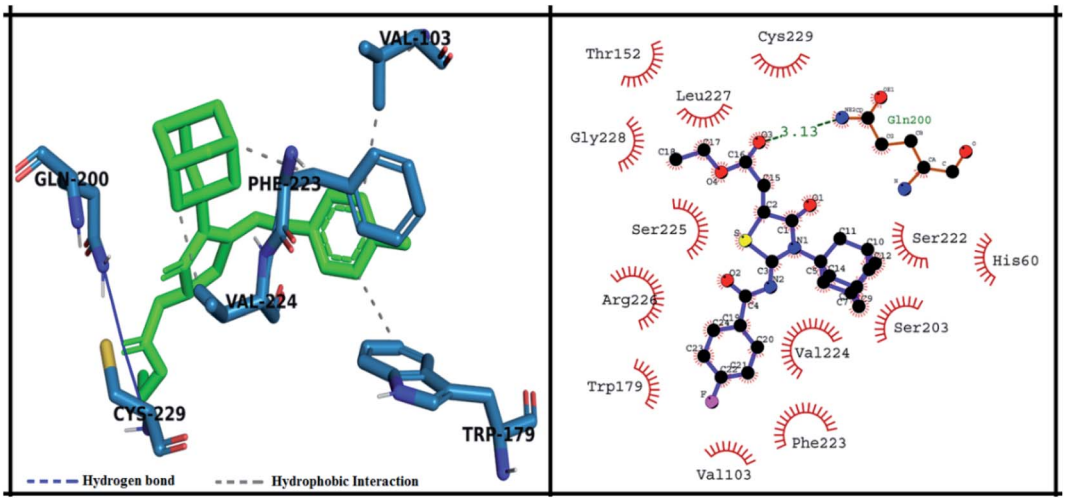

Fig. 7 Putative 2D and 3D binding mode of compound **5a** (green colored) within active pocket of elastase enzyme (amino acid residues in blue color).

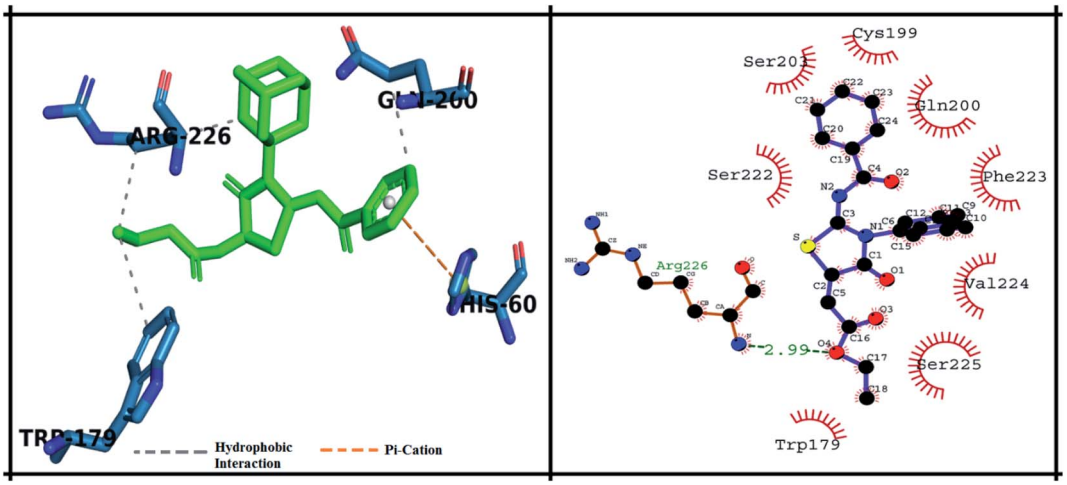

Fig. 8 Putative 2D and 3D binding mode of compound **5f** (green colored) within active pocket of elastase enzyme (amino acid residues in blue color).

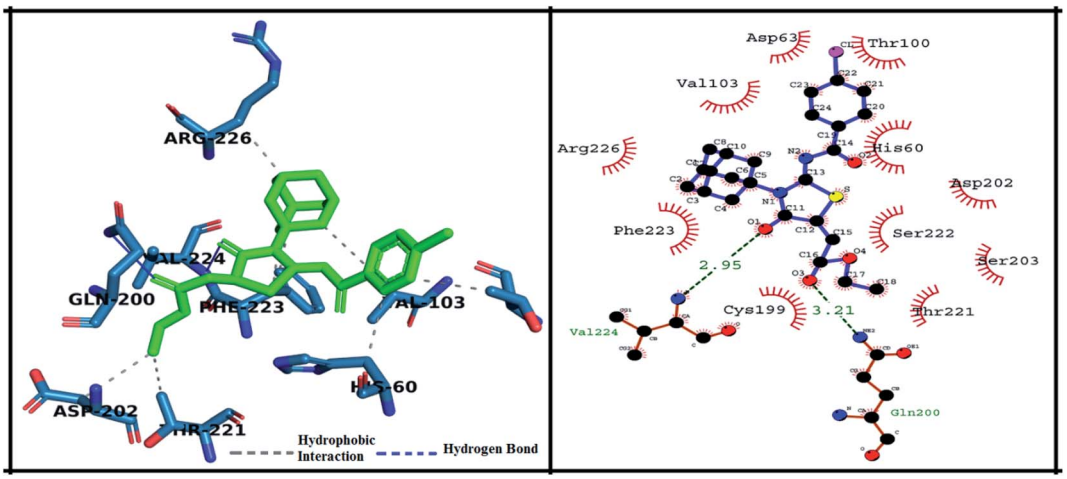

Fig. 9 Putative 2D and 3D binding mode of compound **5g** (green colored) within active pocket of elastase enzyme (amino acid residues in blue color).

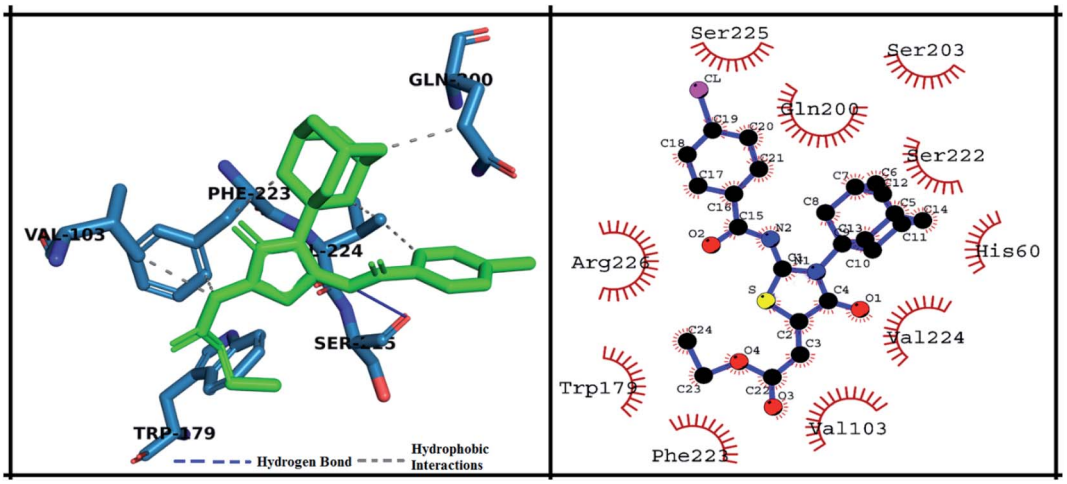

Fig. 10 Putative 2D and 3D binding mode of compound **5h** (green colored) within active pocket of elastase enzyme (amino acid residues in blue color).

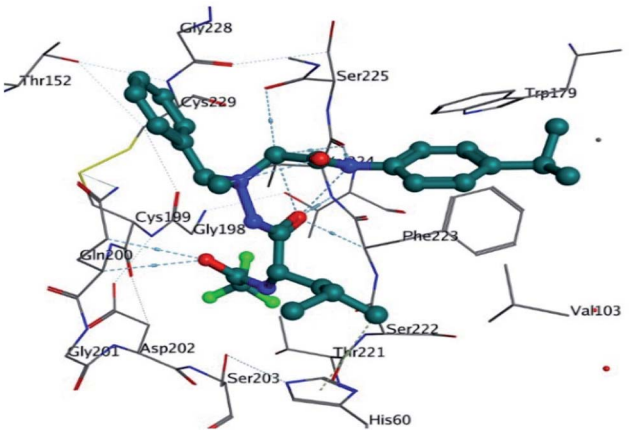

Fig. 11 Putative binding interactions of the co crystal ligand with in the active pocket of porcine pancreatic elastase enzyme.

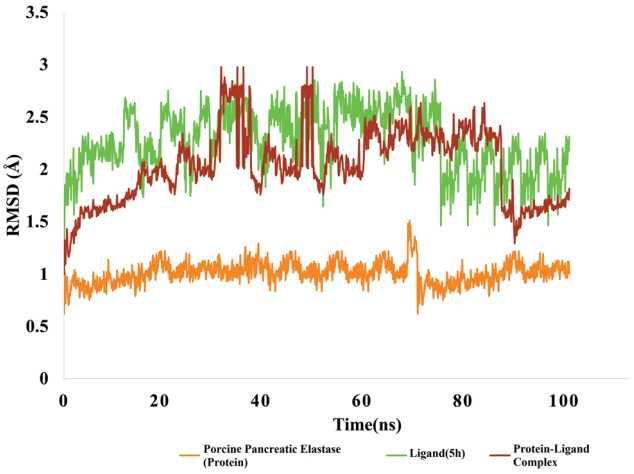

Fig. 12 RMSD value of protein (porcine pancreatic elastase), compound **5h** and protein–ligand complex.

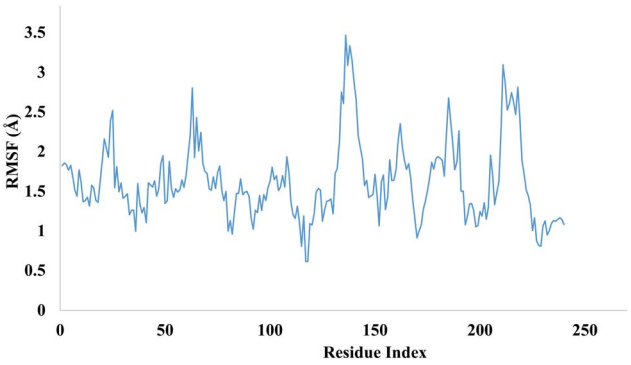

Fig. 13 Evolution of RMSF value for targeted protein.

and drug development. *In silico* ADMET evaluation models were developed to assist the scientist in drug design and lead optimization. Physicochemical properties, absorption, distribution, metabolism, toxicity, excretion, and medicinal properties of adamantyl hybrid iminothiazolidinones derivatives are calculated through the online web server ADMET lab 2.0. It is an integrated online platform for accurate and comprehensive prediction of ADMET properties. ADMET factors that were considered are physicochemical properties, blood–brain barrier (BBB), Caco-2 permeability, volume of distribution (VD), *P*-glycoprotein (PGP) substrate, *P*-glycoprotein (PGP) substrate, plasma protein binding, human intestinal absorption (HIA), MDCK permeability, clearance (CL), half-life ($T_{1/2}$), eye corrosion, eye irritation, respiratory toxicity, AMES toxicity, carcinogenicity, and synthetic accessibility score.

Total ten adamantyl hybrid iminothiazolidinones derivative were subjected ADMET study using online web server ADMETlab 2.0. It was observed that physicochemical properties of all compounds were meeting the criteria of drug like rule *i.e.*, Lipinski rule of five (Table 6).

Moreover, it was observed that all compounds showed a positive value of Caco-2 permeability. Caco-2 permeability is

Table 5 Hydrogen observed during MD simulations

S. no.	Donor	Acceptor
1	VAL224-main	**5h**-side
2	**5h**-side	GLN200-side
3	GLN200-side	**5h**-side
4	ARG64-side	**5h**-side
5	**5h**-side	LEU227-main
6	**5h**-side	ARG226-main
7	TYR170-side	**5h**-side
8	ARG36-side	**5h**-side
9	SER39-side	**5h**-side
10	GLY38-main	**5h**-side
11	**5h**-side	ASN153-side
12	**5h**-side	SER225-main
13	THR44-side	**5h**-side

human colon epithelial cell line which corresponds to better human intestinal absorption. A drug having a Caco-2+ value corresponds to high intestinal absorption. The calculated value for human intestinal absorption (HIA) showed that all compounds have probability of good absorption from intestinal membrane. Furthermore, the calculated value for human intestinal absorption was better than standard oleanolic acid for compound **5h** and **5i**. A compound having positive value of blood–brain barrier have better lipophilicity profile and it can absorb readily from plasma membranes. Calculated values for blood–brain barrier (BBB) and blood placental barriers (BPB) for all compounds were found to be better than standard. It was noticed that the compounds **5a**, **5d**, **5h** and **5i** showed better lipophilicity profile and values was observed as BBB++. In terms of Plasma glycoprotein (PGP) substrate and PGP-inhibitor, it was observed that the output value of all compounds had the probability of being PGP-substrate, and PGP-inhibitor. Plasma protein binding (PPB) is an important factor to determine safety of drugs, as drug having high value of PPB (>90%) have narrow therapeutic index whereas drugs having low value of PPB are much safer. In the present study, compounds **5b**, **5c**, **5f**, **5g**, and **5j** showed low PPB values, which means that these compounds have a broad therapeutic index. In terms of carcinogenicity, compounds **5f**, **5h**, and **5i** were found to be non-carcinogenic whereas all other compounds have the probability of being carcinogenic. AMES toxicity profile depicted that compounds have probability of being toxic. Synthetic accessibility score (SA score) is designed to estimate ease of synthesis of drug-like molecules, and it was observed that all compounds have positive value of SA score. Overall, all compounds showed better ADMET profile, all values are tabulated in Table 7 given below.

Experimental

General information

Solvent and reagents were purchased from Sigma-Aldrich and dried before use. The melting point was finding a digital Gallenkamp (SANYO) model MPD BM 3 apparatus and was uncorrected. ^{1}H NMR and ^{13}C NMR spectra were determined in $CDCl_3$ or acetone-d_6 solutions at 300 MHz and 75.4 MHz, respectively using a Bruker AM-300 spectrophotometer. FTIR spectra were recorded using an FTS 3000 MX spectrophotometer. The chemical shifts were measured in ppm units and coupling constants (J) in hertz.

Synthesis of the compounds

Substituted aryl carboxylic acid (3.97 mmol, 1.2 mol eq.) was reacted with thionyl chloride (4.30 mmol, 1.3 mol eq.) under inert conditions at reflux in dichloromethane. When the reaction was completed, the dichloromethane was removed under reduced pressure. The resulting acid chloride was converted to isothiocyanate by adding potassium thiocyanate (4.96 mmol, 1.5 mol eq.) in acetone. Amantadine (3.31 mmol, 1 mol eq.) was added to the reaction mixture and heated to 40 °C for 1.5 hours. The reaction mixture was pure in crushed ice the crude product precipitated out and recrystallized in ethanol. The obtained acyl thioureas (1.27 mmol, 1 mol eq.) was further reacted with ethyl 4-ethoxypent-4-en-2-ynoate (2.54 mmol, 2 mol eq.) at room temperature. The final product precipitated out during reaction. The product was filtered, dried, recrystallized in ethanol. Other compounds were prepared using the same method.

Ethyl (*Z*)-2-((*Z*)-3-((3s,5s,7s)-adamantan-1-yl)-2-((2-methylbenzoyl)imino)-4-oxothiaz olidin-5-ylidene)acetate (5a). White solid: yield: 88%; R_f: 0.6; mp 173–176 °C; IR: 2980, 2907, 2849 (aliphatic C–H stretching), 1715, 1697, 1639 (3C═O), 1540 (N═C), 1257 (C–S) cm^{-1}. ^{1}H NMR: (300 MHz, $CDCl_3$, 300 MHz) δ ppm, 8.14 (d, 1H, $J = 7.5$ Hz, Ar-H), 7.45 (t, 1H, $J = 6.9$, 7.5 Hz, Ar-

Table 6 Physiochemical properties of the compounds (**5a–j**)

Physicochemical properties								
	Molecular weight	Density	*n*HA	*n*HD	TPSA	log *S*	log *P*	log *D*
5a	452.18	0.999	6	0	76.04	−6.135	4.727	4.124
5b	452.18	0.999	6	0	76.04	−6.157	4.704	4.416
5c	468.17	1.014	7	0	85.27	−5.992	4.502	4.201
5d	516.07	1.135	6	0	76.04	−6.378	5.05	4.34
5e	472.12	1.048	6	0	76.04	−6.282	4.922	4.502
5f	456.15	1.033	6	0	76.04	−6.0	4.519	4.195
5g	438.16	1.006	6	0	76.04	−5.78	4.413	4.182
5h	472.12	1.048	6	0	76.04	−6.177	4.937	4.09
5i	472.12	1.048	6	0	76.04	−6.28	4.626	4.288
5j	468.17	1.014	7	0	85.27	−6.013	4.466	4.179

Table 7 ADMET profile of the compounds (**5a–j**)

Absorption & distribution properties

	Volume of distribution (VD)		Human intestinal absorption (HIA)		Caco-2 permeability		Blood brain barrier (BBB) & blood-placenta barrier (BPB)		Plasma protein binding (PPB)		PGP-Inhibitor		*p*-Glycoprotein substrate (PGP-substrate)		MDCK Permeability	
Mode	Result	Probability	Result	Probability	Result	Probability	Result	Probability	Result	Probability	Result	Probability	Result	Probability	Result	Probability
5a	++	0.609	+	0.023	+	−4.564	++	0.596	−	95.90%	+	0.003	+	0.0	+	6.3×10^{-5}
5b	+	0.621	+	0.04	+	−4.622	+	0.738	+	85.93%	+	0.016	+	0.001	+	2.7×10^{-5}
5c	+	0.572	+	0.108	+	−4.607	+	0.799	+	84.80%	+	0.013	+	0.001	+	2.4×10^{-5}
5d	++	0.795	+	0.136	+	−4.593	++	0.495	−	95.43%	+	0.237	+	0.001	+	2.3×10^{-5}
5e	+	0.707	+	0.012	+	−4.571	+	0.516	−	95.67%	+	0.035	+	0.001	+	4.3×10^{-5}
5f	+	0.595	+	0.026	+	−4.568	+	0.741	+	86.58%	+	0.026	+	0.001	+	2.7×10^{-5}
5g	+	0.618	+	0.036	+	−4.605	+	0.799	+	82.55%	+	0.01	+	0.001	+	3.2×10^{-5}
5h	+	0.624	+	0.01	+	−4.532	++	0.313	−	98.30%	+	0.033	+	0.0	+	6.4×10^{-5}
5i	+	1.052	+	0.012	+	−4.615	++	0.136	−	99.81%	+	0.611	+	0.001	+	2.8×10^{-5}
5j	+	0.58	+	0.079	+	−4.599	+	0.77	+	85.15%	+	0.011	+	0.001	+	2.2×10^{-5}

Metabolism / Excretion

	CYP1A2 Inhibitor		CYP2C19 Inhibitor		CYP2C9 Inhibitor		CYP2D6 Inhibitor		CYP3A4 Inhibitor		CL		$T_{1/2}$	
	Result	Probability	Result	Probability	Result	Probability	Result	Probability	Result	Probability	Result	Probability	Result	Probability
5a	Inh	0.173	Inh	0.872	Inh	0.933	Inh	0.167	Inh	0.497	Low	3.831	Long	0.006
5b	Inh	0.167	Inh	0.872	Inh	0.918	Inh	0.07	Inh	0.416	Low	3.263	Long	0.016
5c	Inh	0.215	Inh	0.886	Inh	0.944	Inh	0.056	Inh	0.589	Low	4.483	Long	0.018
5d	Inh	0.216	Inh	0.823	Inh	0.908	Inh	0.063	Inh	0.276	Low	1.328	Long	0.008
5e	Inh	0.265	Inh	0.867	Inh	0.935	Inh	0.157	Inh	0.388	Low	2.767	Long	0.012
5f	Inh	0.213	Inh	0.84	Inh	0.886	Inh	0.054	Inh	0.286	Low	3.103	Long	0.006
5g	Inh	0.247	Inh	0.875	Inh	0.927	Inh	0.089	Inh	0.376	Low	3.146	Long	0.016
5h	Inh	0.253	Inh	0.847	Inh	0.912	Inh	0.278	Inh	0.316	Low	2.461	Long	0.007
5i	Inh	0.211	Inh	0.866	Inh	0.942	Inh	0.154	Inh	0.418	Low	2.311	Long	0.005
5j	Inh	0.174	Inh	0.855	Inh	0.932	Inh	0.025	Inh	0.413	Low	4.229	Long	0.014

Medicinal properties / Toxicity

	Synthetic accessibility score		Lipinski rule		AMES toxicity		Carcinogenicity		Eye corrosion		Eye irritation		Respiratory toxicity	
	Result	Probability	Result	Probability	Result	Probability	Result	Probability	Result	Probability	Result	Probability	Result	Probability
5a	+	4.078	+	Accepted	+	0.017	+	0.526	+	0.003	+	0.031	+	0.022
5b	+	4.079	+	Accepted	+	0.006	+	0.313	+	0.003	+	0.046	+	0.025
5c	+	4.061	+	Accepted	+	0.006	+	0.209	+	0.003	+	0.044	+	0.024
5d	+	4.086	+	Accepted	+	0.007	+	0.443	+	0.003	+	0.049	+	0.025
5e	+	4.091	+	Accepted	+	0.006	+	0.278	+	0.003	+	0.025	+	0.029

Table 7 (*Contd.*)

	Medicinal properties				Toxicity									
	Synthetic accessibility score		Lipinski rule		AMES toxicity		Carcinogenicity		Eye corrosion		Eye irritation		Respiratory toxicity	
	Result	Probability	Result	Probability	Result	Probability	Result	Probability	Result	Probability	Result	Probability	Result	Probability
5f	+	4.049	+	Accepted	+	0.005	−	0.425	+	0.003	+	0.032	+	0.04
5g	+	4.009	+	Accepted	+	0.008	+	0.292	+	0.003	+	0.063	+	0.03
5h	+	4.045	+	Accepted	+	0.007	−	0.459	+	0.003	+	0.018	+	0.025
5i	+	4.081	+	Accepted	+	0.016	−	0.935	+	0.003	+	0.019	+	0.101
5j	+	4.02	+	Accepted	+	0.007	+	0.257	+	0.003	+	0.038	+	0.025

	TOX21 pathway							
	NR-AR		NR-AR-LBD		NR-ER		Antioxidant response element	
	Result	Probability	Result	Probability	Result	Probability	Result	Probability
5a	Active	0.002	Active	0.027	Active	0.117	Active	0.906
5b	Active	0.001	Active	0.308	Active	0.261	Active	0.972
5c	Active	0.001	Active	0.583	Active	0.28	Active	0.932
5d	Active	0.001	Active	0.347	Active	0.285	Active	0.928
5e	Active	0.0	Active	0.355	Active	0.265	Active	0.94
5f	Active	0.0	Active	0.439	Active	0.199	Active	0.921
5g	Active	0.0	Active	0.484	Active	0.269	Active	0.935
5h	Active	0.001	Active	0.024	Active	0.244	Active	0.915
5i	Active	0.001	Active	0.561	Active	0.286	Active	0.913
5j	Active	0.001	Active	0.599	Active	0.129	Active	0.933

H), 7.33–7.29 (m, 2H, J = 8.1 Hz, Ar-H), 6.82 (s, 1H, C=CH), 4.31 (q, 2H, J = 9 Hz, CH_2), 2.78–2.72 (m, 8H, CH_3, CH_2 adamantyl), 2.28 (s, 3H, CH adamantyl), 1.85–1.72 (m, 6H, CH_2), 1.35 (t, 3H, J = 7.2 Hz). ^{13}C NMR: (75 MHz, $CDCl_3$, 300 MHz) δ ppm, 177.8 (C=O of benzoyl), 166.3 (C=O of ester), 165.6 (C=O), 163.4 (C=N of imine), 141.9 (α, β C=C) 141.5, 133.7, 132.4, 132.1, 131.3 (Ar-C), 125.7 (α, β C=C), 118.1 ((Ar-C)), 67.96 (CH_2), 61.6, 39.7, 36.1, 30.3 (adamantyl), 22.2 (CH_3-Ar), 14.2 (CH_3). HRMS (ESI): calculated for $C_{25}H_{28}N_2O_4S^+$: 453.1770. Found m/z 453.1750 $[M + H]^+$.

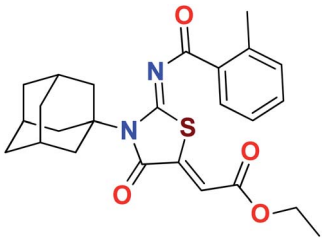

Ethyl (*Z*)-2-((*Z*)-3-((3s,5s,7s)-adamantan-1-yl)-2-((3-methylbenzoyl) imino)-4-oxothiazolidin-5-ylidene)acetate (5b). White solid: yield: 86%; R_f: 0.59; mp 177–179 °C; IR: 2980, 2907, 2847 (aliphatic C–H stretching), 1719, 1693, 1638 (3C=O), 1525 (N=C), 1272 (C–S) cm^{-1}. ^{1}H NMR (300 MHz, $CDCl_3$, 300 MHz) δ ppm, 8.21 (s, 1H, Ar-H), 8.10 (d, 1H, J = 7.8 Ar-H), 7.58 (d, 1H, J = 7.8 Ar-H), 7.45 (t, 1H, J = 7.8 Ar-H), 6.87 (s, 1H, C=CH), 4.31 (q, 2H, J = 9 Hz, CH_2), 2.78–2.72 (m, 8H, CH_3, CH_2 adamantyl), 2.28 (s, 3H, CH adamantyl), 1.85–1.72 (m, 6H, CH_2), 1.35 (t, 3H, J = 7.2 Hz). HRMS (ESI): calculated for $C_{25}H_{28}N_2O_4S^+$: 453.1770. Found m/z 453.1753 $[M + H]^+$.

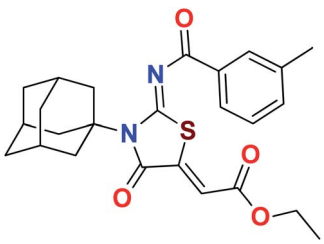

Ethyl (*Z*)-2-((*Z*)-3-((1s,3s)-adamantan-1-yl)-2-((3-methoxybenzoyl)imino)-4 oxothiazolidin-5-ylidene) acetate (5c). White solid: yield: 82%; R_f: 0.58; mp 235–237 °C; IR: 2906 (aliphatic C–H stretching), 1709, 1638, 1613 (3C=O), 1526 (N=C), 1276 (C–S) cm^{-1}. ^{1}H NMR: (300 MHz, $CDCl_3$, 300 MHz) δ ppm, 7.81 (d, 1H, J = 7.5 Hz, Ar-H), 7.73 (d, 1H, J = 2.4 Hz, Ar-H), 7.41 (t, 1H, J = 8.1 Hz, Ar-H), 7.16 (dd, 1H, J = 7.8, 2.1 Hz, Ar-H), 6.85 (s, 1H, C=CH), 4.31 (q, 2H, J = 9 Hz, CH_2), 3.89 (s, 3H, O– CH_3), 2.77 (d, 6H, J = 2.4 Hz, CH_2, adamantyl), 2.26 (s, 3H, CH adamantyl), 1.80 (q, 6H, J = 12 Hz, CH_2 adamantyl), 1.35 (t, 3H, J = 7.2 Hz, CH_3). ^{13}C NMR (75 MHz, $CDCl_3$, 300 MHz) δ ppm, 176.3 (C=O of benzoyl), 166.5 (C=O of ester), 165.8 (C=O), 165.4 (C=N of imine), 159.7 (Ar-C), 141.6 (α, β C=C), 136.4 (Ar-C), 129.5 (α, β C=C), 122.6, 120.2, 118.7, 113.9 (Ar-C), 68.2 (CH_2), 61.6, 55.4 (O–CH_3), 39.7, 36.1, 30.4, 14.2 (CH_3). HRMS (ESI): calculated for $C_{25}H_{28}N_2O_5S^+$: 469.1719. Found m/z 469.1714 $[M + H]^+$.

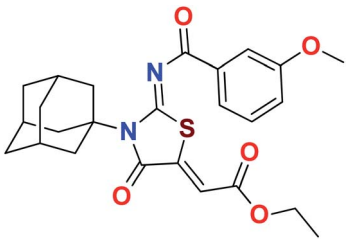

Ethyl (*Z*)-2-((*Z*)-3-((3s,5s,7s)-adamantan-1-yl)-2-((4-bromobenzoyl) imino)-4-oxothiazolidin-5-ylidene) acetate (5d). White solid: yield: 85%; R_f: 0.52; mp 181–183 °C; IR: 3057, 2905, 2848 (aliphatic C–H stretching), 1721, 1691, 1650 (3C=O), 1509 (N=C), 1265 (C–S) cm^{-1}.^{1}H NMR (300 MHz, $CDCl_3$, 300 MHz) δ ppm, 8.07 (d, 2H, J = 8.7 Hz, Ar-H), 7.65 (d, 2H, J = 8.7 Hz, Ar-H), 6.86 (s, 1H, C=CH), 4.32 (q, 2H, J = 7.2 Hz, CH_2), 2.75 (d, 6H, J = 2.4 Hz, CH_2, adamantyl), 2.26 (s, 3H, CH adamantyl), 1.80 (q, 6H, J = 12.3 Hz, CH_2, adamantyl), 1.36 (t, 3H, J = 7.2 Hz, CH_3). ^{13}C NMR (75 MHz, $CDCl_3$, 300 MHz) δ ppm, 175.6 (C=O of benzoyl), 166.9 (C=O of ester), 166.4 (C=O), 165.4 (C=N of imine), 141.4 (α, β C=C), 134.1, 131.9, 131.5. HRMS (ESI): calculated for $C_{24}H_{25}BrN_2O_4S^+$: 517.0718. Found m/z 517.0715 $[M + H]^+$.

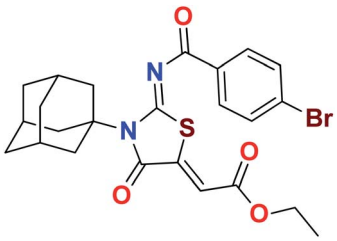

Ethyl (*Z*)-2-((*Z*)-3-((3s,5s,7s)-adamantan-1-yl)-2-((3-chlorobenzoyl) imino)-4-oxothiazolidin-5-ylidene) acetate (5e). White solid: yield: 75%; R_f: 0.50; mp 193–194 °C; IR: 2977, 2914, 2848 (aliphatic C–H stretching), 1724, 1692, 1637 (3C=O), 1519 (N=C), 1287 (C–S) cm^{-1}. ^{1}H NMR (300 MHz, $CDCl_3$, 300 MHz) δ ppm, 8.21 (s, 1H, Ar-H) 8.08 (d, 1H, J = 7.8 Ar-H), 7.57 (d, 1H, J = 7.8 Ar-H), 7.45 (t, 1H, J = 7.8 Ar-H), 6.87 (s, 1H, C=CH), 4.32 (q, 2H, J = 7.2 Hz, CH_2), 2.77 (s, 6H, CH_2, adamantyl), 2.28 (s, 3H, CH adamantyl), 1.82–1.80 (q, 6H, J = 12.3 Hz, CH_2, adamantyl), 1.36 (t, 3H, J = 7.2 Hz, CH_3), ^{13}C NMR (75 MHz, $CDCl_3$, 300 MHz) δ ppm, 175.1 (C=O of benzoyl), 167.4 (C=O of ester), 166.4 (C=O), 165.4 (C=N of imine), 141.3 (α, β C=C), 136.9, 134.7, 133.2, 130.2 (Ar-C), 129.9 (α, β C=C), 119.2 (Ar-C), 113.9 (Ar-C), 68.5 (CH_2), 61.7, 39.7, 36.1, 30.4, 14.2 (CH_3). HRMS (ESI): calculated for $C_{24}H_{25}ClN_2O_4S^+$: 473.1224. Found m/z 473.1219 $[M + H]^+$.

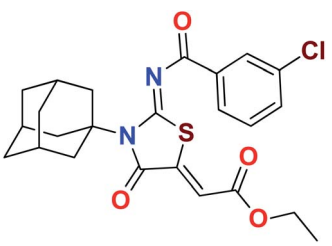

Ethyl (*Z*)-2-((*Z*)-3-((3s,5s,7s)-adamantan-1-yl)-2-((4-fluorobenzoyl) imino)-4-oxothiazolidin-5-ylidene) acetate (5f). White crystalline solid: yield: 87%; R_f: 0.48; mp 231–233 °C; IR: 2980, 2907, 2850 (aliphatic C–H stretching), 1719, 1697, 1639 (3C=O), 1535 (N=C), 1270 (C–S) cm^{-1}. ^1H NMR (300 MHz, $CDCl_3$, 300 MHz) δ ppm, 8.25–8.20 (dd, 2H, J = 5.4 Hz, J = 8.7 Hz,Ar-H) 7.21–7.15 (t, 2H, J = 8.7 Hz, Ar-H), 6.85 (s, 1H, C=CH), 4.31 (q, 2H, J = 7.2 Hz, CH_2), 2.76 (s, 6H, CH_2, adamantyl), 2.26 (s, 3H, CH adamantyl), 1.86–1.74 (q, 6H, J = 12.3 Hz, CH_2, adamantyl), 1.35 (t, 3H, J = 7.2 Hz, CH_3), ^{13}C NMR (75 MHz, $CDCl_3$, 300 MHz) δ ppm, 175.2 (C=O of benzoyl), 167.7 (C=O of ester), 166.4 (C=O), 165.4 (C=N of imine), 164.3 (Ar-C) 141.5 (α, β C=C),132.6, 132.5, 131.1 (α, β C=C), 118.9, 115.9, 115.6 (Ar-C), 68.2 (CH_2), 61.7, 39.7, 36.1, 30.3, 14.2 (CH_3). HRMS (ESI): calculated for $C_{24}H_{25}FN_2O_4S^+$: 457.1519. Found m/z 457.1517 $[M + H]^+$.

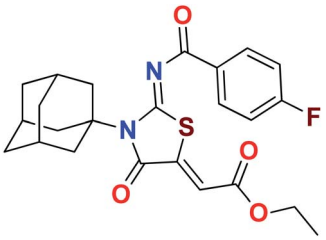

Ethyl (*Z*)-2-((*Z*)-3-((3s,5s,7s)-adamantan-1-yl)-2-(benzoylimino)-4-oxothiazolidin-5-ylidene) acetate (5g). White solid: yield: 89%; R_f: 0.61; mp 167–169 °C; IR: 2979, 2913, 2848 (aliphatic C–H stretching), 1719, 1697, 1634 (3C=O), 1530 (N=C), 1270 (C–S) cm^{-1}. ^1H NMR (300 MHz, $CDCl_3$, 300 MHz) δ ppm, 8.21 (d, 2H, J = 7.9 Hz, Ar-H), 7.64–7.59 (tt, 1H, J = 7.8 Hz, J = 1.2 Hz Ar-H), 7.51 (t, 2H, J = 7.8 Hz, Ar-H), 6.85 (s, 1H, C=CH), 4.31 (q, 2H, J = 9 Hz, CH_2), 2.77 (d, 6H, J = 2.4 Hz, CH_2, adamantyl), 2.26 (s, 3H, CH adamantyl), 1.80 (q, 6H, J = 12 Hz, CH_2 adamantyl), 1.35 (t, 3H, J = 7.2 Hz, CH_3). ^{13}C NMR (75 MHz, $CDCl_3$, 300 MHz) δ ppm, 176.4 (C=O of benzoyl), 166.5 (C=O of ester), 165.7 (C=O), 165.4 (C=N of imine), 141.6 (α, β C=C), 135, 133.4, 130 (Ar-C), 128.6 (α, β C=C), 118.7 (Ar-C), 68.2 (CH_2), 61.7, 39.7, 36.1, 30.4, 14.2 (CH_3). HRMS (ESI): calculated for $C_{24}H_{26}N_2O_4S^+$: 439.1613. Found m/z 439.1610 $[M + H]^+$.

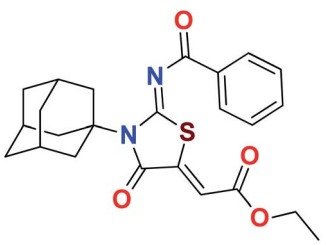

Ethyl (*Z*)-2-((*Z*)-3-((3s,5s,7s)-adamantan-1-yl)-2-((4-chlorobenzoyl) imino)-4-oxothiazolidin-5-ylidene) acetate (5h). White solid: yield: 81%; R_f: 0.49; mp 181–183 °C; IR: 2980, 2908, 2849 (aliphatic C–H stretching), 1721, 1699, 1639 (3C=O), 1535 (N=C), 1269 (C–S) cm^{-1}. ^1H NMR (300 MHz, $CDCl_3$, 300 MHz) δ ppm, 8.15 (dd, 2H, J = 6.9 Hz, J = 1.8 Hz Ar-H), 7.49 (dd, 2H, J = 6.6 Hz, J = 1.8 Hz Ar-H), 6.87 (s, 1H, C=CH), 4.31 (q, 2H, J = 9 Hz, CH_2), 2.76 (d, 6H, J = 2.4 Hz, CH_2, adamantyl), 2.26 (s, 3H, CH adamantyl), 1.80 (q, 6H, J = 12 Hz, CH_2 adamantyl), 1.35 (t, 3H, J = 7.2 Hz, CH_3). ^{13}C NMR (75 MHz, $CDCl_3$, 300 MHz) δ ppm, 175.5 (C=O of benzoyl), 166.9 (C=O of ester), 166.4 (C=O), 165.4 (C=N of imine), 141.6 (α, β C=C), 139.8, 133.6, 131.3 (Ar-C), 128.9 (α, β C=C), 119.1 (Ar-C), 68.3 (CH_2), 61.7, 39.7, 36.1, 30.4, 14.2 (CH_3). HRMS (ESI): calculated for $C_{24}H_{25}ClN_2O_4S^+$: 473.1224. Found m/z 473.1220 $[M + H]^+$.

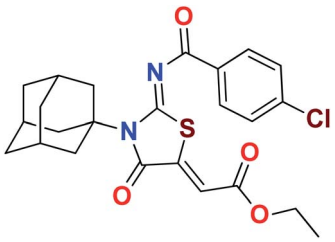

Ethyl (*Z*)-2-((*Z*)-3-((3s,5s,7s)-adamantan-1-yl)-2-((2-chlorobenzoyl) imino)-4-oxothiazolidin-5-ylidene) acetate (5i). White solid: yield: 79%; R_f: 0.63; mp 166–167 °C; IR: 2984, 2906, 2849 (aliphatic C–H stretching), 1724, 1697, 1646 (3C=O), 1533 (N=C), 1256 (C–S) cm^{-1}. ^1H NMR (300 MHz, $CDCl_3$, 300 MHz) δ ppm, 8.02 (dd, 1H, J = 7.5 Hz, J = 1.5 Hz Ar-H), 7.51–7.35 (m, 3H, Ar-H), 6.87 (s, 1H, C=CH), 4.31 (q, 2H, J = 9 Hz, CH_2), 2.71 (d, 6H, J = 2.4 Hz, CH_2, adamantyl), 2.22 (s, 3H, CH adamantyl), 1.75 (q, 6H, J = 12 Hz, CH_2 adamantyl), 1.35 (t, 3H, J = 7.2 Hz, CH_3). ^{13}C NMR (75 MHz, $CDCl_3$, 300 MHz) δ ppm, 175.7 (C=O of benzoyl), 166.3 (C=O of ester), 165.4 (C=O), 165.2 (C=N of imine), 141.2 (α, β C=C), 134.3, 134, 132.7, 131.8, 131.4 (Ar-C), 126.6 (α, β C=C), 118.1 (Ar-C), 68.3 (CH_2), 61.7, 39.6, 36, 30.3, 14.2 (CH_3). HRMS (ESI): calculated for $C_{24}H_{25}ClN_2O_4S^+$: 473.1224. Found m/z 473.1222 $[M + H]^+$.

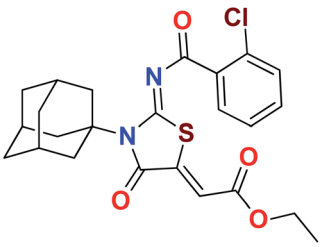

Ethyl (*Z*)-2-((*Z*)-3-((3s,5s,7s)-adamantan-1-yl)-2-((4-methoxybenzoyl) imino)-4-oxothiazolidin-5-ylidene) acetate (5j). White solid: yield: 83%; R_f: 0.58; mp 211–213 °C; IR: 2944, 2896, 2842 (aliphatic C–H stretching), 1703, 1638, 1602 (3C=O), 1535 (N=C), 1247 (C–S) cm^{-1}. ^1H NMR (300 MHz, $CDCl_3$, 300 MHz) δ ppm, 8.17 (d, 2H, J = 8.7 Hz, Ar-H), 6.82 (d, 2H, J = 8.7, Ar-H), 6.83 (s, 1H, C=CH), 4.30 (q, 2H, J = 9 Hz, CH_2), 3.90 (s, 3H, O–CH_3), 2.76 (d, 6H, J = 2.4 Hz, CH_2, adamantyl), 2.26 (s, 3H, CH adamantyl), 1.80 (q, 6H, J = 12 Hz, CH_2 adamantyl), 1.34 (t, 3H, J = 7.2 Hz, CH_3). ^{13}C NMR (75 MHz, $CDCl_3$, 300 MHz) δ ppm, 175.7 (C=O of benzoyl), 166.5 (C=O of ester), 165.4 (C=O), 164.8 (C=N of imine), 163.9 (Ar-C), 141.9 (α, β C=C), 132.3 (Ar-C), 127.8 (α, β C=C), 118.4, 113.8 (Ar-C), 68 (CH_2), 61.6, 55.5 (O–CH_3), 39.7, 36.2, 30.4, 14.2 (CH_3). HRMS (ESI): calculated for $C_{25}H_{28}N_2O_5S^+$: 469.1719. Found m/z 469.1717 $[M + H]^+$.

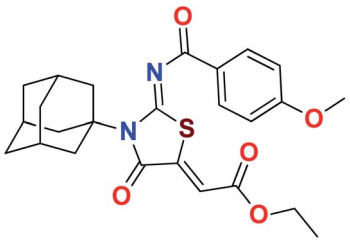

In vitro methodology

Elastase inhibition assay. The inhibition activity of elastase (elastase from porcine pancreas) was determined by following the methods of ref. 34 and 35 with minor modifications as discussed in our previously reported article.[36] By measuring the absorbance of the solution at 410 nm, the amount of released *p*-nitroaniline, which had been hydrolyzed by the substrate (*N*-succinyl-Ala-Ala-Ala-*p*-nitroanilide), could be used to determine the elastase inhibition activity. It was necessary to prepare a 0.8 mM solution of the *N*-succinyl-Ala-Ala-Ala-*p*-nitroanilide in a 0.2 M Tris–HCl buffer in order to conduct the experiment (pH 8.0). The buffer solution (130 μL) was added to the test sample (10 μL) in a 96-well microplate, and the mixture was mixed thoroughly. The microplate was pre-incubated for 10 minutes at 25 °C before the addition of an commercially available elastase stock solution (10 mL, 0.0375 unit per mL) was performed. Following the addition of the enzyme, the microplate was maintained at 25 °C for 30 minutes, and the absorbance at 410 nm was measured using a microplate reader (SpectraMax ABS, USA). The IC_{50} values were determined through the series of triplicate experiments with eight different concentrations as a serial dilution using default protocol in the SoftMax pro software. Using the following formula, it was possible to calculate the elastase inhibition activities:

$$\text{Elastase inhibition activity (\%)} = (OD_{control} - OD_{sample} \times 100)/OD_{control}$$

where $OD_{control}$ and OD_{sample} represents the optical densities in the absence and presence of sample, respectively. Oleanolic acid was used as the standard inhibitor for elastase. The IC_{50} of the derivatives was calculated by assaying the eight different concentrations of the tested derivatives (serial dilutions). The observed values were analyzed through non-linear calculations using graph pad prism software 5 as discussed in previously reported article.[35]

Protocol for kinetics

To determine the mode of inhibition, a kinetic analysis was performed using our previously published method[34] in the following manner: the compound **5g** was chosen based on its high IC_{50} value and high potency. It was possible to study the kinetics of compound **5g** by varying the concentration of *N*-succinyl-Ala-Ala-Ala-*p*-nitroanilide in the presence of various concentrations of compound **5g** (0.00, 0.062, 0.124, and 0.248 μM). Briefly, the *N*-succinyl-Ala-Ala-Ala-*p*-nitroanilide concentration was changed from 2, 1, 0.5, 0.25, 0.125, and 0.0625 mM for kinetics studies, and the rest of the procedure was the same as described in the elastase inhibition assay protocol. The maximum initial velocities were determined from the initial linear portion of absorbance up to 10 minutes after the addition of the enzyme at a rate of one minute intervals until the enzyme was removed. The type of inhibition on the enzyme was determined by plotting the inverse of velocities ($1/V$) against the inverse of substrate concentration $1/[S]$ mM^{-1} on a Lineweaver–Burk plot. SoftMaxPro was used to process the data after it was collected. An analysis of a secondary plot of $1/V$ against inhibitor concentration revealed that the E_I dissociation constant K_i was observed.

Computational studies

Quantum chemistry through density functional theory calculation. The density functional theory (DFT) is one of widely used method to determine the electron density and energetic parameter of the compounds. It is used to determine the structure of atoms, molecules, crystals, surfaces, and their interactions. These calculations are done by using the Gaussian 09W program on the Linux based workstation.[37] B3LYP method was used to determine vibrational wavenumbers with an SVP basis set. It is known that the B3LYP functional assists a good description of harmonic vibrational wavenumbers for small and medium-sized compounds. The optimized structural parameters are further use for calculations. The output check files were analyzed by GuassView 6.0.[38]

Molecular docking studies. Molecular docking studies were performed using Molecular Operating Environment (MOE) 2015.10 software package.[39] The docking studies were conducted to evaluate and investigate binding energies and binding affinities of synthesized derivatives within activation loop of targeted protein. The crystallographic structure of targeted protein porcine pancreatic elastase (PDB ID = 1 BMA; resolution 1.99 angstrom) was obtained from protein data bank (https://www.rcsb.org/).[40] All the steps for protein preparation that are pre requisite for docking procedure were performed. Initially co-crystal ligand and het atoms were removed moreover, water molecules were also removed as they interfere with ligand molecules during docking calculations. The addition of polar hydrogen atoms with their standard 3D geometry, addition of partial Gasteiger charges using MMFF94x as a force field was undertaken. Furthermore, fixation of errors in connections, repairing missing residues, 3D protonation, and fixation of potential and energy minimization was also performed using protein preparation wizard of MOE software. The selection of same active site amino acid residues of co crystal inhibitor was carried out using site finder utility of MOE 2015.10. Dummies atoms were created at the site of selected amino acid residues. The structures synthesized thiazolidinone derivatives (**5a–j**) were generated using Chemdraw ultra 12.0. The generated structures were optimized to steepest energy gradient prior to docking with targeted protein. The ligand database comprising of synthesized thiazolidinone derivatives were docked into selected amino acid residues of active site. Docking protocol was as follows, placement method was set to triangular

matcher, scoring methodology was set to London dG, refinement methodology was set to rigid receptor and GBVI/WSA dG was the scoring function for selection of best pose from 100 poses for each compound. After completion of docking protocol, best poses for each compound were evaluated for their fittings into active pocket and best protein–ligand conformations were selected on the basis of docking score for further analysis. The analysis and visualization of best docked pose was carried out using PyMol.[41] The putative 2D ligand interactions were created using LigPlot$^+$ 2.2.[42] It is run from intuitive java interface which provide detailed 2D interactions of protein–ligand complex. Molecular docking protocol was validated by re-docking co-crystal ligand benzyl methyl aminimide inhibitor with amino acid residues of active site.

ADMET properties. Determination of biochemical processes from drug administration to elimination plays a vital role in lead optimization. An ideal drug candidate should be administered and absorbed into the systemic circulation and must be non-toxic and eliminate without affecting the biological activity. These processes are seeming to be distinct, but they are closely inter-related, so the determination of ADMET properties have prime importance in the drug discovery process. Since traditional methods were time-consuming and much research till 1990 went into vain due to the appearance of undesirable effects in the middle of the drug discovery process. So, the determination of ADMET properties is of prime importance to rolling out undesired effects of a drug candidate at the initial stage of the drug discovery process. Efficient and reliable online prediction models developed for *in silico* determination of ADMET properties. ADMET properties like absorption, distribution, metabolism, excretion, toxicity and physicochemical properties of eight compounds were done using online *in silico* prediction model ADMET lab 2.0.[43] All compounds were converted to SMI format using ChemDraw Ultra and these SMI structures were loaded into online server ADMET lab 2.0. It also facilitates the manually generating the desired structures using JMSE editor.

Molecular dynamic simulations. The molecular dynamic study of top ranked conformation was performed using Nano scale molecular dynamic (NAMD) software[44] on CUDA-accelerated GPU system having 16 core processor and 64 GB RAM memory. Visualization of MD simulations was carried out using VMD software.[45] MD simulations were carried out in order to determine binding interactions and stability of protein–ligand complex under accelerated conditions. Top ranked protein–ligand complex was selected and topology files were generated for protein and ligand using CHARMM36 forcefield.[46] The system was neutralized by addition of NaCl charges. The system was minimized to steepest-energy gradient to remove any close contacts between atoms. The system was equilibrated in NVT ensemble for 500 000 steps followed by equilibration in NPT ensemble for additional 500 000 steps. Afterward, simulation was performed for 100 ns under periodic boundaries condition.[47] The calculation of binding energy, van der Waals and electrostatic interactions were carried out using PME method.[48]

Conclusions

A structurally diverse series of adamantyl-iminothiazolidinone conjugates was synthesized, characterized, and tested for *in vitro* elastase inhibition assay and subjected to *in silico* ADMET prediction. The inhibition studies revealed compounds **5a**, **5f**, **5g**, and **5h** to show significant activity. Compound **5g** with no substitution on benzoyl ring having IC_{50} value (IC_{50} 0.124 μM) elastase was 50 times more potent as compared to oleanolic acid having IC_{50} 5.996 μM. Kinetic studies showed competitive mode of inhibition and excellent binding energies. Overall, all compounds showed better ADMET profile, indicating their potential to serve as lead compounds in drug discovery. The comprehensive *in silico* studies including molecular docking studies, drug likeness properties and stability of top ranked protein–ligand complex was conducted to evaluate and support *in vitro* studies. All these studies suggested potent inhibitory potential of synthesized derivatives.

Conflicts of interest

The authors declare no conflict of interests.

Acknowledgements

The authors gratefully acknowledge the Quaid-i-Azam University for environment conducive for research.

References

1 A. Janoff, *Annu. Rev. Med.*, 1985, **36**(1), 207–216.
2 P. Guilloteau, R. Zabielski and J. W. Blum, *Physiol. Pharmacol.*, 2009, **60**, 37–46.
3 C. Dumont, C. Bourgeois, H. Fessi, P. Y. Dugas and V. Jannin, *Int. J. Pharm.*, 2019, **565**, 409–418.
4 D. C. Whitcomb and M. E. Lowe, *Dig. Dis. Sci.*, 2007, **52**(1), 1–17.
5 D. M. Goldberg, *Clin. Chim. Acta*, 2000, **291**(2), 201–221.
6 N. Arshad, M. Rafiq, R. Ujan, A. Saeed, S. I. Farooqi, F. Perveen, P. A. Channar, S. Ashraf, Q. Abbas, A. Ahmed and T. Hokelek, *RSC Adv.*, 2020, **10**(35), 20837–20851.
7 P. A. Henriksen, *Curr. Opin. Hematol.*, 2014, **21**(1), 23–28.
8 E. S. Al-Abdullah, H. H. Asiri, S. Lahsasni, E. E. Habib, T. M. Ibrahim and A. A. El-Emam, *Drug Des., Dev. Ther.*, 2014, **8**, 505–518.
9 J. Liu, D. Obando, V. Liao, T. Lifa and R. Codd, *Eur. J. Med. Chem.*, 2011, **46**, 1949–1963.
10 A. Saeed, U. Flörke and M. F. Erben, *J. Mol. Struct.*, 2014, **1065**, 150–159.
11 L. Wanka, K. Iqbal and P. R. Schreiner, *Chem. Rev.*, 2013, **113**(5), 3516–3604.
12 G. Lamoureux and G. Artavia, *Curr. Med. Chem.*, 2010, **17**(26), 2967–2978.
13 L. L. Gladkov, S. V. Gaponenko, E. V. Shabunya-Klyachkovskaya, A. N. Shimko, E. S. Al-Abdullah and A. A. El-Emam, *Spectrochim. Acta Mol. Biomol. Spectrosc.*, 2014, **128**, 874–879.

14 F. J. Jiménez-Jiménez, H. Alonso-Navarro, E. García-Martín and J. A. G. Agúndez, *J. Pers. Med.*, 2020, **10**(4), 217.
15 F. J. Jiménez-Jiménez, H. Alonso-Navarro, E. García-Martín and J. A. G. Agúndez, *J. Pers. Med.*, 2020, **10**(4), 217.
16 S. R. Brenner, *J. Med. Virol.*, 2020, **92**(11), 2341–2342.
17 R. F. Butterworth, *J. Parkinsons Dis.*, 2020, **7**(1), 4.
18 E. Wolf, K. Seppi, R. Katzenschlager, G. Hochschorner, G. Ransmayr, P. Schwingenschuh, E. Ott, I. Kloiber, D. Haubenberger and M. D. Auff, *Mov. Disord.*, 2010, **25**(10), 1357–1363.
19 U. Zahra, S. Zaib, A. Saeed, M. ur Rehman, G. Shabir, H. O. Alsaab and I. Khan, *Int. J. Biol. Macromol.*, 2021, **198**, 157–167.
20 N. Arshad, A. Saeed, F. Perveen, R. Ujan, S. I. Farooqi, P. A. Channar, G. Shabir, H. R. El-Seedi, A. Javed and M. Yamin, *Bioorg. Chem.*, 2021, **109**, 104707.
21 H. Aziz, A. Saeed, M. A. Khan, S. Afridi and F. Jabeen, *Mol. Diversity*, 2021, **25**(2), 763–776.
22 S. Parveen, K. K. Tong, M. Khawar Rauf, M. Kubanik, M. A. Shaheen, T. Söhnel, S. M. Jamieson, M. Hanif and C. G. Hartinger, *Chem.–Asian J.*, 2019, **14**(8), 1262–1270.
23 V. Kshtriya, B. Koshti, D. K. Pandey, S. Kharbanda, D. K. Singh, D. Bhatia and N. Gour, *R. Soc. Chem. Spec. Publ.*, 2021, **17**(16), 4304–4316.
24 A. Kalaiyarasi, J. Haribabu, D. Gayathri, K. Gomathi, N. Bhuvanesh, R. Karvembu and V. Biju, *J. Mol. Struct.*, 2019, **1185**, 450–460.
25 R. K. Mohapatra, P. K. Das, M. K. Pradhan, M. M. El-Ajaily, D. Das, H. F. Salem, U. Mahanta, G. Badhei, P. K. Parhi and A. A. Maihub, *Comments Mod. Chem.*, 2019, **39**(3), 127–187.
26 H. Nkabyo, G. Bosman, R. Luckay and K. Koch, *Inorg. Chim. Acta*, 2020, **508**, 119644.
27 A. M. Plutin, R. Ramos, R. Mocelo, A. Alvarez, E. E. Castellano, M. R. Cominetti, K. M. Oliveira, T. D. de Oliveira, T. E. Silva and R. S. Correa, *Polyhedron*, 2020, **184**, 114543.
28 T. Parvin, R. Yadav and L. H. Choudhury, *Org. Biomol. Chem.*, 2020, **18**(29), 5513–5532.
29 J. Balzarini, B. Orzeszko-Krzesińska, J. K. Maurin and A. Orzeszko, *Eur. J. Med. Chem.*, 2009, **41**(1), 303–311.
30 S. Ashraf, A. Saeed, S. H. Moon, U. Flörke, S. H. Kim, Z. Ashraf, M. Yaseen and M. Latif, *J. Med. Chem.*, 2020, **5**(13), 3965–3970.
31 S. Ali, A. Saeed, N. Abbas, M. Shahid, M. Bolte and J. Iqbal, *MedChemComm*, 2012, **3**(11), 1428–1434.
32 M. S. Weiss, S. Panjikar, E. Nowak and P. A. Tucker, *Acta Crystallogr., Sect. D: Biol. Crystallogr.*, 2002, **58**, 1407–1412.
33 G. Hansen, H. Gielen-Haertwig, P. Reinemer, D. Schomburg, A. Harrenga and K. Niefind, *MedChemComm*, 2011, **409**, 681–691.
34 R. Mathammal, N. Jayamani and N. Geetha, *J. Spectrosc.*, 2013, 171735.
35 A. Saeed, S. A. Ejaz, A. Ul-Hamid, H. R. El-Seedi and J. Iqbal, *J. Mol. Struct.*, 2021, 130821.
36 R. A. Costa, E. S. A. Junior, J. d. A. Bezerra, J. M. Mar, E. S. Lima, M. L. B. Pinheiro, D. V. Mendonça, G. B. P. Lopes, A. D. S. Branches and K. M. Oliveira, *J. Chem.*, 2019, 9627404.
37 M. J. Frisch, G. W. Trucks, H. B. Schlegel, G. E. Scuseria, M. A. Robb, J. R. Cheeseman, G. Scalmani, V. Barone, B. Mennucci, G. A. Petersson, *et al.*, *Gaussian09, R. A. J. I.*, Gaussian Inc., Wallingford C. T., 2009, 121, pp. 150–166.
38 R. Dennington, T. A. Keith, and J. M. Millam, *GaussView, Version 6*, Semichem Inc., Shawnee Mission, KS, 2016.
39 *MOE (Molecular Operating Environment), Version 2015.10*, Chemical Computing Group.
40 S. K. Burley, H. M. Berman, G. J. Kleywegt, J. L. Markley, H. Nakamura and S. Velankar, *Methods Mol. Biol.*, 2017, 627–641.
41 S. Yuan, H. S. Chan and Z. Hu, *Wiley Interdiscip. Rev.: Comput. Mol. Sci.*, 2017, **7**, e1298.
42 R. A. Laskowski and M. B. Swindells, *J. Chem. Info. Model.*, 2011, **51**(10), 2778–2786.
43 *ADMETlab 2.0*, **https://admetmesh.scbdd.com/**, accessed 29 September 2021.
44 J. C. Phillips, D. J. Hardy, J. D. Maia, J. E. Stone, J. V. Ribeiro, R. C. Bernardi, R. Buch, G. Fiorin, J. Hénin and W. Jiang, *J. Chem. Phys.*, 2020, **153**, 044130.
45 W. Humphrey, A. Dalke and K. Schulten, *J. Mol. Graphics*, 1996, **14**, 33–38.
46 S. Kim, J. Lee, S. Jo, C. L. Brooks III, H. S. Lee and W. Im, *J. Comput. Chem.*, 2017, **38**, 1879–1886.
47 P. L. Barclay and D. Z. Zhang, *J. Comput. Phys.*, 2021, **435**, 110238.
48 E. K. Guckel, *Large scale simulations of particulate systems using the PME method*, University of Illinois at Urbana-Champaign, 1999.